

Switchable and tunable triple-channel bandpass filter

Ming-En Tian(田明恩), Zhi-He Long(龙之河), Li-Jun Feng(冯丽君), Lei-Lei He(贺磊磊), and Tian-Liang Zhang(张天良)

Citation: Chin. Phys. B, 2022, 31 (**7**): 078401. DOI: 10.1088/1674-1056/ac4f4f
Journal homepage: http://cpb.iphy.ac.cn; http://iopscience.iop.org/cpb

What follows is a list of articles you may be interested in

Switchable down-, up- and dual-chirped microwave waveform generation with improved time-bandwidth product based on polarization modulation and phase encoding

Yuxiao Guo(郭玉箫), Muguang Wang(王目光), Hongqian Mu(牟宏谦), and Guofang Fan(范国芳)
Chin. Phys. B, 2022, 31 (**7**): 078404. DOI: 10.1088/1674-1056/ac5982

A high rectification efficiency $Si_{0.14}Ge_{0.72}Sn_{0.14}$–$Ge_{0.82}Sn_{0.18}$–Ge quantum structure n-MOSFET for 2.45 GHz weak energy microwave wireless energy transmission

Dong Zhang(张栋), Jianjun Song(宋建军), Xiaohuan Xue(薛笑欢), and Shiqi Zhang(张士琦)
Chin. Phys. B, 2022, 31 (**6**): 068401. DOI: 10.1088/1674-1056/ac339e

Theoretical and experimental study on frequency pushing effect of magnetron

Kang Li(李慷), Yi Zhang(张益), Hua-Cheng Zhu(朱铧丞), Ka-Ma Huang(黄卡玛), Yang Yang(杨阳)
Chin. Phys. B, 2019, 28 (**11**): 118402. DOI: 10.1088/1674-1056/ab4d3d

Modeling and experimental studies of a side band power re-injection locked magnetron

Wen-Jun Ye(叶文军), Yi Zhang(张益), Ping Yuan(袁萍), Hua-Cheng Zhu(朱铧丞), Ka-Ma Huang(黄卡玛), Yang Yang(杨阳)
Chin. Phys. B, 2016, 25 (**12**): 128402. DOI: 10.1088/1674-1056/25/12/128402

Cubature Kalman filters： Derivation and extension

Zhang Xin-Chun, Guo Cheng-Jun
Chin. Phys. B, 2013, 22 (**12**): 128401. DOI: 10.1088/1674-1056/22/12/128401

Switchable and tunable triple-channel bandpass filter

Ming-En Tian(田明恩)[1], Zhi-He Long(龙之河)[2], Li-Jun Feng(冯丽君)[1], Lei-Lei He(贺磊磊)[1], and Tian-Liang Zhang(张天良)[1,†]

[1] *School of Aeronautics and Astronautics, University of Electronic Science and Technology of China, Chengdu* 611731, *China*
[2] *Department of Mechanical Engineering, City University of Hong Kong, Kowloon, Hong Kong SAR, China*

(Received 20 November 2021; revised manuscript received 18 January 2022; accepted manuscript online 27 January 2022)

A triple-channel bandpass filter with switchable and tunable functions is proposed, which is based on a triple-mode cross resonator. The varactors and switching diodes are loaded at the end of the resonator. Because of the use of switches, resonators have four working states: conventional single-mode, two dual-modes, and one triple-mode. The varactor makes the channel independently adjustable. Finally, a triple-channel bandpass filter with switchable and tunable functions is designed by using two identical triple-mode resonator coupling structures. To solve the problem of whether each channel in the multi-channel filter is independently adjustable, this paper gives a simple and rigorous judgment method, namely rank criterion, which is a necessary and sufficient condition for each channel to be independently adjustable. The method of designing an element variable coupling matrix (EVCM) is adopted, which can not only obtain the desired frequency response through adjustable elements but also help to select resonators and coupling modes in the actual circuit design. The final circuit size of the designed filter is $0.29\lambda g \times 0.26\lambda g$. The measured results are in good agreement with the simulation results.

Keywords: independently adjustable, switchable, triple-channel

PACS: 84.30.Vn, 84.40.Dc **DOI:** 10.1088/1674-1056/ac4f4f

1. Introduction

Compared with the traditional fixed filter, a reconfigurable filter shows great advantages by supporting a variety of standards and operation modes in the system through its fast adjustment of center frequency and bandwidth. Besides, the reconfigurable filter can adapt to the high frequency band like the fixed filter.[1,2] Especially in recent years, with the development of wireless communication technology and remote sensing system, multiplexers and multichannel filters with reconfigurable performance have become a research hotspot. Taken into consideration in the multi-channel filter with fixed frequency is only the coupling between resonators and external feeding at several fixed frequency points, so it is easy to achieve.[3,4] For a dual-channel filter designed in Refs. [5,6], only the low-frequency channel has reconfigurable performance. Because the two modes constituting the high-frequency channel are not controlled by the varactor. In Ref. [7], a dual-channel filter is designed by using two pairs of $\lambda/4$ uniform microstrip lines loaded with varactor diodes. The magnetic coupling is introduced by punching holes between the resonators, which not only saves the varactor used to control the interstage coupling but also forms a cascaded quadruplet model with the introduced cross electrical coupling to generate a pair of transmission zeros,thereby greatly improving the selectivity of the passband. In Ref. [8], a balanced feed is added into two tunable filters working at low frequency and high frequency respectively and thus obtaining a better in-band reflection. In Ref. [9], the filter has the characteristics of dual-passband and dual-stopband by loading switching diodes on the main transmission line.

Although the filters in Refs. [7–9] have obvious advantages in passband selectivity, in-band reflection, and multi-function, they all use single-mode resonators to design two independent channels, which is not conducive to the miniaturization of devices. In Refs. [10–12], a compact dual-channel reconfigurable filter is designed by using a dual-mode resonator loaded with varactors. In Ref. [13], a dual-channel independently adjustable filter is designed using a ring multimode resonator, and a low-pass filter is cascaded to improve the high-end suppression. Although in Refs. [7–13] the dual-channel reconfigurable filters have been implemented, there is no channel selection function, and the two channels can work only at the same time. In Refs. [14,15], the extreme voltage is applied to the varactor to make a corresponding channel be in a serious impedance mismatch state, thereby realizing the channel selection function. In Refs. [16,17] the authors made the function of filter channel selection more stable and reliable by loading switching diodes.

In this paper, a switchable and tunable triple-channel bandpass filter is proposed. By loading switching diodes and varactor diodes on a cross resonator, the filter has four states: one single channel, two dual-channels, and one triple-channel, and each channel is reconfigurable in these four states. Finally, the varactor is also loaded at the external feed to make the external Q of the filter changeable and broaden the tunable range of the passband.

[†]Corresponding author. E-mail: ztl@uestc.edu.cn

© 2022 Chinese Physical Society and IOP Publishing Ltd

2. Design of reconfigurable filter

Figure 1(a) shows the layout of the switchable and tunable triple-channel bandpass filter presented in this paper. The core is a triple-mode cross resonator as shown in Fig. 1(b), which is the evolution of the cross resonator. Translating the lower branch to the left d_1 enables channel 3 to obtain the appropriate coupling strength, which will be described in detail below.

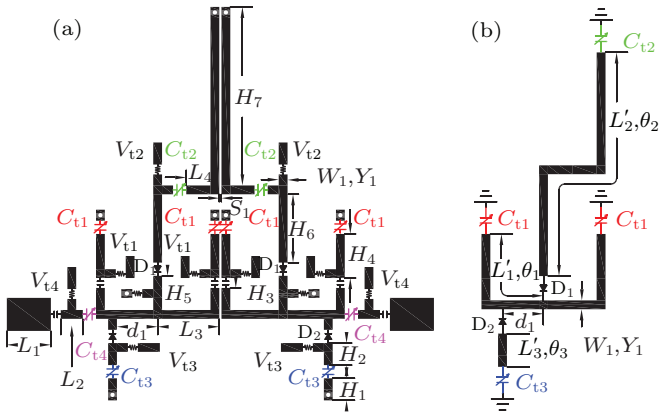


Fig. 1. Layout of (a) filter and (b) resonator.

Because the offset d_1 is small, the resonator can still be regarded as an approximately symmetrical structure, and the odd–even mode analysis method is still applicable to the resonator. The resonator is not only loaded with a varactor at the end of the microstrip line but also embedded with two switching diodes. When switching diodes D_1 and D_2 are off, the resonator is a single-mode f_1 resonator, and the equivalent circuit is shown in Fig. 2(a). When the switching diode D_1 is on and D_2 is off, the resonator is a T-shaped dual-mode resonator. According to the odd–even mode analysis method, the corresponding odd mode f_o equivalent circuit and even mode f_{e1} equivalent circuit can be obtained as shown in Figs. 2(b) and 2(c) respectively. When the switching diode D_1 is off and D_2 is on, the resonator is also a T-shaped dual-mode resonator. The corresponding odd mode f_o equivalent circuit and even mode f_{e2} equivalent circuit are shown in Figs. 2(b) and 2(d) respectively. When the switch diode D_1 and D_2 are both on, the resonator is a triple-mode cross resonator, and the corresponding odd mode and even mode equivalent circuits are shown in Figs. 2(b)–2(d).

Two resonators in Fig. 1(b) are arranged in parallel as shown in Fig. 1(a), and the coupling between the same modes can form three channels. As the filter is schematically shown in Fig. 3, Channel 1 is formed at low frequency f_{e1}, channel 2 is generated at middle frequency f_o or f_1, and channel 3 is created at high frequency f_{e2}. Therefore, when the switching diodes D_1 and D_2 are both off, only channel 2 works, which is a single channel state. When the switching diode D_1 is on and D_2 is off, both channel 1 and channel 2 work, which is in the dual-channel state. When the switching diode D_1 is off and D_2 is on, both channel 2 and channel 3 work, which is also a dual-channel state. When the switching diodes D_1 and D_2 are both on, channel 1, channel 2, and channel 3 work, which is in the triple-channel state. The corresponding relationship between switching mode and channel number is shown in Table 1.

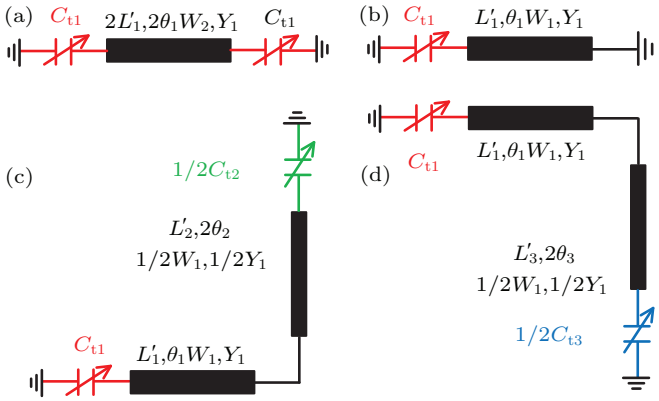


Fig. 2. (a) Single mode f_1 resonator, (b) odd mode f_o resonator, (c) even mode f_{e1} resonator, and (d) even mode f_{e2} resonator.

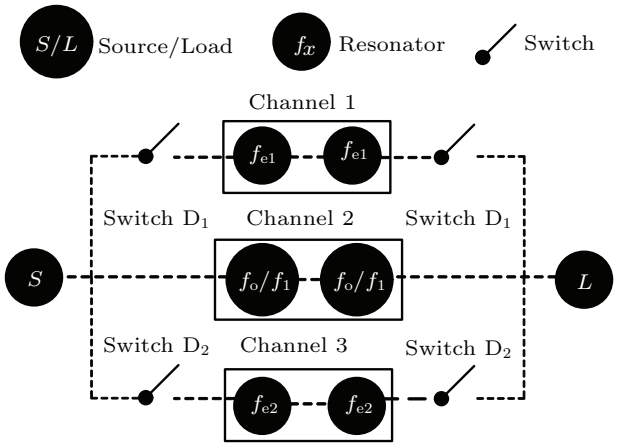


Fig. 3. Schematic diagram of switchable and tunable triple-channel bandpass filter.

The center frequencies of the three channels of the filter designed in this paper are set to be 0.7 GHz, 1.5 GHz, and 2.5 GHz. The thickness of the substrate is 1 mm, the dielectric constant is 2.2, the microstrip linewidth W_1 is 0.8 mm and the admittance Y_1 is 0.01 S. According to the transmission line theory, the resonance conditions of the four equivalent circuits in Fig. 2 can be obtained and expressed as Eqs. (1)–(4).

Table 1. Corresponding switch and channel number.

Switch number \ Channel number	Single-channel	Dual-channel		Triple-channel
	f_1	f_{e1} & f_o/f_o & f_{e2}		f_{e1}&f_o & f_{e2}
D_1	OFF	ON	OFF	ON
D_2	OFF	OFF	ON	ON

$$2\tan^{-1}\left(\frac{2\pi f_1 C_{t1}}{Y_1}\right)+2\left(\frac{2\pi f_1\sqrt{\varepsilon_r}L_1'}{c}\right)=\pi, \tag{1}$$

$$\tan^{-1}\left(\frac{2\pi f_o C_{t1}}{Y_1}\right)+\frac{2\pi f_o\sqrt{\varepsilon_r}L_1'}{c}=\frac{\pi}{2}, \tag{2}$$

$$\tan^{-1}\left(\frac{2\pi f_{e1} C_{t1}}{Y_1}\right)+\frac{2\pi f_{e1}\sqrt{\varepsilon_r}(L_1'+L_2')}{c}+\tan^{-1}\left(\frac{2\pi f_{e1} C_{t2}}{Y_1}\right)=\pi, \tag{3}$$

$$\tan^{-1}\left(\frac{2\pi f_{e2} C_{t1}}{Y_1}\right)+\frac{2\pi f_{e2}\sqrt{\varepsilon_r}(L_1'+L_3')}{c}+\tan^{-1}\left(\frac{2\pi f_{e2} C_{t3}}{Y_1}\right)=\pi. \tag{4}$$

The transmission line theory used here involves mainly the resonance condition, input admittance and electrical length of the resonator. The electric length of the fundamental frequency of the $\lambda/2$ resonator and the $\lambda/4$ resonator are π and $\pi/2$, respectively. Then, according to the forms of the four resonators in Figs. 2, figures 2(a), 2(c), and 2(d) can be classified as $\lambda/2$ resonator, figure 2(b) is classified as $\lambda/4$ resonator. Then, the capacitance is transformed into an equivalent microstrip line by means of the input admittance formula, so that the equivalent electrical length of the resonator can be acquired.

According to formulas (1) and (2), $f_1 = f_o$, C_{t1} takes a middle value of the adjustable range of varactor capacitance value of 1.5 pF, $f_1 = f_o = 1.5$ GHz, and then they are substituted into formula (1) or (2) to obtain an initial value of L_1', 12.8 mm. Similarly, C_{t2} takes a middle value of the variable capacitance diode changeable range, 20 pF, $f_{e1} = 0.7$ GHz, $L_1' = 12.8$ mm and then they are substituted into formula (3) to obtain the initial value of L_2', 36.7 mm. The C_{t3} takes a middle value of the tunable range of varactor capacitance 1 pF, $f_{e2} = 2.5$ GHz, $L_1' = 12.8$ mm, and then they are substituted into formula (4) to obtain the initial value of L_3' as 0.7 mm.

After the initial value of the resonator is obtained, the variation trends of the transmission poles with the capacitance of the varactor can be obtained according to formulas (1)–(4). When $C_{t2} = C_{t3} = 0.5$ pF, the resonant frequencies f_1, f_{e1}, f_o, and f_{e2} decrease with the augment of the varactor C_{t1}, indicating that C_{t1} has a significant effect on f_1, f_{e1}, f_o, and f_{e2}. When $C_{t1} = 0.5$ pF, the resonant frequencies f_{e1} and f_{e2} decrease with the augment of varactor C_{t2} and C_{t3}, but f_o and f_1 remain unchanged. It shows that C_{t2} and C_{t3} have an effect on f_{e1} and f_{e2}, but not on f_o nor f_1. According to the odd–even mode equivalent circuit diagram in Fig. 2 and the variation trend of transmission poles with varactor in Fig. 4, C_{t1} can control three channels by affecting f_{e1}, f_o, and f_{e2} resonant modes, C_{t2} can control channel 1 by affecting f_{e1} mode, and C_{t3} can control channel 3 by affecting f_{e2} mode. Table 2 shows the corresponding relationship between the varactor and the channel. In Table 2, number 1 indicates that the varactor can control the channel, and number 0 represents that the varactor cannot control the channel, and then matrix A can be obtained from Table 2 as shown in formula (5).

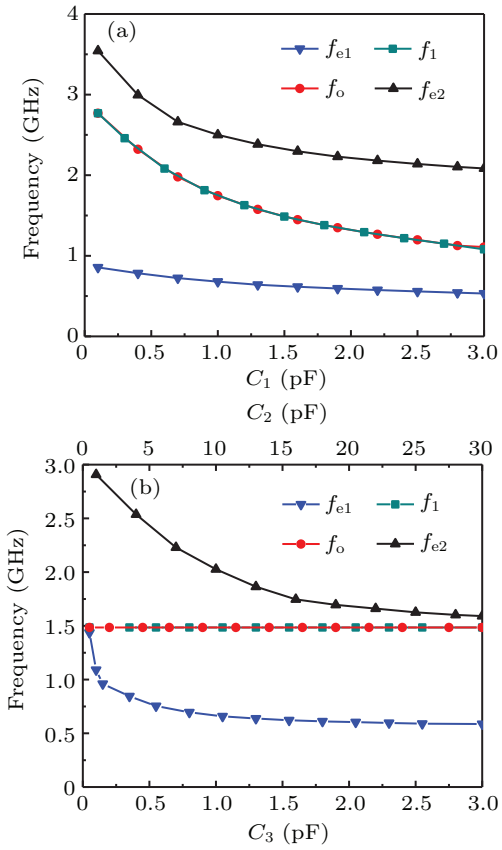


Fig. 4. Variation trend of transmission pole with capacitance of varactor, indicating (a) change trend of transmission pole with varactor C_{t1} when $C_{t2} = C_{t3} = 0.5$ pF, and (b) the change trend of transmission pole with varactor C_{t2} and C_{t3} when $C_{t1} = 0.5$ pF.

Table 2. Corresponding varactors and channels.

	Channel 1 (f_{e1})	Channel 2 (f_o)	Channel 3 (f_{e2})
C_{t1}	1	1	1
C_{t2}	1	0	0
C_{t3}	0	0	1

$$A=\begin{bmatrix}1&1&1\\1&0&0\\0&0&1\end{bmatrix}\xrightarrow{r_1\leftrightarrow r_2}\begin{bmatrix}1&0&0\\1&1&1\\0&0&1\end{bmatrix}\xrightarrow{r_2-r_1}\begin{bmatrix}1&0&0\\0&1&1\\0&0&1\end{bmatrix}\xrightarrow{r_2-r_3}\begin{bmatrix}1&0&0\\0&1&0\\0&0&1\end{bmatrix}=B\Rightarrow R(A)=R(B)=3. \tag{5}$$

The channels of the single-channel filter, dual-channel filter, and triple-channel filter given in this paper each are independently adjustable, which are related to not only the number of varactor loaded but also the loading position. Usually, we first draw the odd-mode and even-mode equivalent circuit of the resonator, then observe the varactor controlling the mode constituting each channel, judge and infer whether each mode can be independently adjustable, and finally conclude whether each channel is independently tunable. However, the more the

channels, the more complex the judgment is, here in this work a simple and rigorous judgment method named rank criterion is given.

Taking a triple-channel filter given in this paper for example, Matrix A can be obtained from Table 2, and matrix B can be obtained through row transformation. Matrix B is a third-order identity matrix with rank 3. Therefore, it can be concluded that if matrix A is a full rank matrix, each channel of the multichannel filter is independently adjustable. Thus, if A is an $m \times n$ matrix, where m is the number of varactor diodes and n is the number of channels, the rank of matrix A is $R(A)$. If $m < n$ or $R(A) < n \leq m$, the multichannel filter must not be independently adjustable for each channel, and the number of channels that can be independently adjustable is $R(A)$. If $R(A) = n \leq m$, the multichannel filter must be independently adjustable for each channel. Therefore, the necessary and sufficient condition for each channel of multichannel filter to be independently adjustable is $R(A) = n \leq m$.

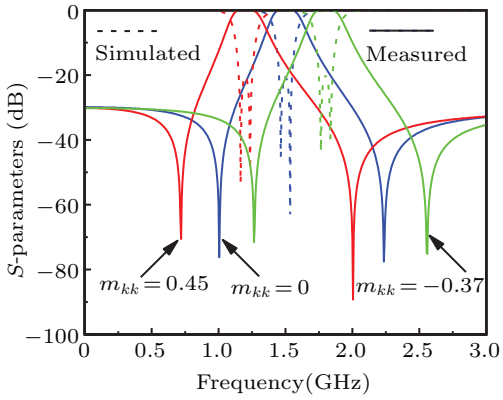


Fig. 5. Response curves according to EVCM.

Reference [15] gives a simple and effective method to design a reconfigurable bandpass filter. The response of the reconfigurable filter can be accurately characterized by the element variable coupling matrix. According to the presetting parameters of the filter (1.2 GHz–1.8 GHz, BW = 150 MHz), the external Q value resonant frequency and coupling coefficient within the reconfigurable range can be obtained to accurately guide the design of the filter. The $[M_\Delta]t$ represents EVCM, the fixed component of matrix $[M_\Delta]t$ is $[M_\Delta]$, m_{kk} is the self-coupling coefficient, $[c]$ is the slope matrix, c_Q is the coefficient of external quality factor Q_e, f_d is the calibration frequency, and f_t is the adjustable center frequency. Take the single channel in this paper for example, according to the element coupling matrix and the presetting tunable range, the frequency response curves can be obtained as shown in Fig. 5. Now, the value of m_{kk} varies in a range from -0.37 to 0.45, and the calibration frequency f_d is 1.5 GHz.

$$[m_\Delta]_t = ([m_\Delta] + m_{kk}[c]), \tag{6}$$

$$Q_{et} = \Delta Q_e + m_{kk} c_Q, \tag{7}$$

$$m_{kk} = f_d/f_t - f_t/f_d, \tag{8}$$

$$[m_\Delta] = \begin{bmatrix} 0 & 0.1692 \\ 0.1692 & 0 \end{bmatrix}, \quad \Delta Q_e = 6.84, \tag{9}$$

$$[c] = \begin{bmatrix} 1 & 0.085 \\ 0.085 & 1 \end{bmatrix}, \quad c_Q = -3.28. \tag{10}$$

The lower branch of the resonator used in this work is shifted leftward by d_1 to regulate the coupling strength between the f_{e2} of the two resonators. It is specified that the left offset of the branch from the midpoint is positive and the right offset is negative. As can be seen from Fig. 6, the coupling strength k of f_{e2} decreases with the increase of the offset d_1 and the gap S_1, indicating that after the gap S_1 is determined, the offset d_1 can be adjusted to effectively control the coupling strength k. After calculating the EVCM, k is obtained to be about 0.06, final gap S_1 0.2 mm, and offset d_1 4 mm.

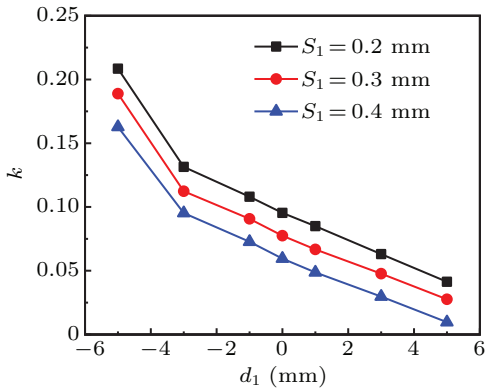


Fig. 6. Variation trend of coupling strength k with offset d_1 under different values of gap S_1.

$$Q_{exe1} = \pi f_{e1} \tau_{S_{11e1}}, \quad Q_{exo} = \pi f_o \tau_{S_{11o}},$$
$$Q_{exe2} = \pi f_{e2} \tau_{S_{11e2}}. \tag{11}$$

To meet the external Q value of the three channels, especially to broaden the reconfigurable ranges of the channels, the switchable and tunable triple-channel bandpass filter proposed in this paper adopts the varactor C_{t4} feed at the port. Figure 7 shows the theoretical external Q values required in the tunable ranges of three channels and the actual external Q values extracted under different C_{t4} values from formula (11). When C_{t4} becomes smaller or the frequency becomes larger, the external Q value of each channel becomes larger. Within the variation range of C_{t4}, the external Q values required by the three channels in their respective regulation range can be fully met. As shown in Fig. 7, the line of theoretical external Q value required by each channel is sandwiched between the external Q value polyline when $C_{t4} = 2.5$ pF and the external Q value polyline when $C_{t4} = 15$ pF. The external Q value required by channel 2 within the adjustable range is analyzed by the EVCM method above. According to formulae (7)–(10), the external Q value is between 5.36 and 8.05. Considering the influence of in-band reflection, the calculation results are basically consistent with the scenarios in Fig. 7(b), which also proves the reliability of the EVCM method.

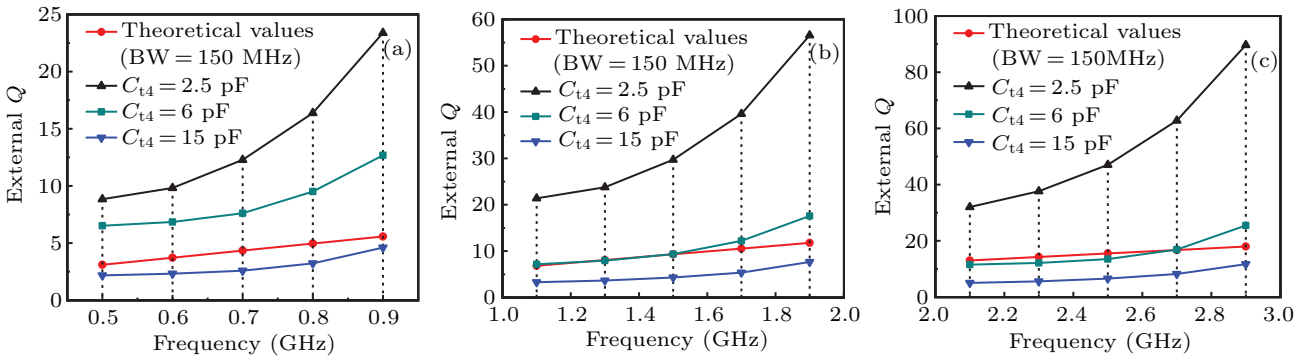


Fig. 7. External Q of (a) channel 1, (b) channel 2, and (c) channel 3.

3. Fabrication and measurements

Finally, the switchable and tunable triple-channel bandpass filter proposed in this paper is processed on the substrate with material F4BM-2, thickness of 1 mm and dielectric constant of 2.2. To prevent it from oxidizing, the circuit surface is plated with gold. The fabricated filter is shown in Fig. 8. According to the marks in Fig. 1(a), the specific dimensions are as follows: $L_1 = 4$ mm, $L_2 = 2$ mm, $L_3 = 5.6$ mm, $L_4 = 4.4$ mm, $H_1 = 2$ mm, $H_2 = 2$ mm, $H_3 = 2$ mm, $H_4 = 3.2$ mm, $H_5 = 3.1$ mm, $H_6 = 6.2$ mm, $H_7 = 16.2$ mm, $W_1 = 0.8$ mm, $S_1 = 0.2$ mm, and $d_1 = 4.1$ mm; the overall size of the circuit is 38.8 mm×35.7 mm (including DC bias circuit), *i.e.*, $0.29\lambda g \times 0.26\lambda g$. All varactor diodes are SMV1405-079LF ($C_j = 0.63$ pF–2.67 pF) for C_{t1}, SMV1273-079LF ($C_j = 2.15$ pF–31.18 pF) for C_{t2} and C_{t4}, and SMV2020-079LF ($C_j = 0.35$ pF–3.2 pF) for C_{t3}. All resistors marked in the figure are 100 kΩ with package 0603, and the marked DC isolation capacitors are 39-pF Murata high Q special capacitors with package 0603.

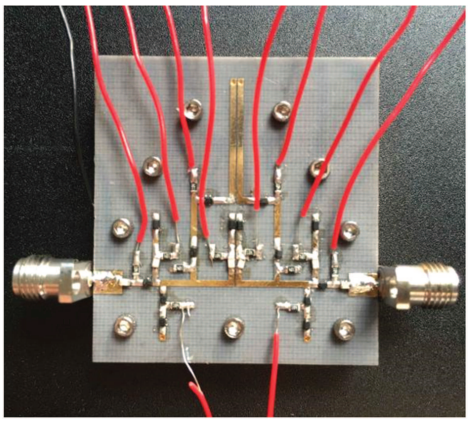


Fig. 8. Fabricated switchable and tunable triple-channel bandpass filter.

Figure 9 displays the simulation and measurement results of the filter which shows that both switches D_1 and D_2 are both off. At this time, it is a single channel filter with a bandwidth of 150 MHz, an adjustment range from 1.27 GHz to 1.85 GHz, in-band reflection better than −15 dB, and there is a transmission zero point on the left and right side of the passband, which greatly improves the channel selectivity. Figure 9(b) shows that switches D_1 and D_2 are both on. At this time, it is a triple-channel filter. The low-frequency channel bandwidth is 200 MHz, the tunable range is between 0.46 GHz and 0.8 2GHz, the middle channel bandwidth is 200 MHz, the reconfigurable range is between 1.37 GHz and 1.71 GHz, the high-frequency channel bandwidth is 150 MHz, the changeable range is between 2.22 GHz and 2.70 GHz, and the reflection of the three channels is better than −13 dB. Figures 9(c) and 9(d) show the switch D_1 is on and D_2 is off. At this time, it is a dual-channel filter. When the high-frequency channel in Fig. 9(c) is located at 1.62 GHz and the bandwidth is 150 MHz, the low-frequency channel bandwidth is 200 MHz, the tunable range is between 0.50 GHz and 0.86 GHz, and the in-band reflection of both channels is better than −13 dB. When the low-frequency channel in Fig. 9(d) is located at 0.65 GHz and the bandwidth is 200 MHz, the high-frequency channel bandwidth is 200 MHz, and the changeable range is between 1.41 GHz and 1.81 GHz. The in-band reflection of both channels is better than −13 dB.

Figures 9(e) and 9(f) show that switch D_1 is off and D_2 is on. At this time, it is also a dual-channel filter. When the high-frequency channel in Fig. 9(e) is located at 2.37 GHz and the bandwidth is 150 MHz, the low-frequency channel bandwidth is 200 MHz and the adjustment range is between 1.32 GHz and 1.57 GHz. The in-band reflection of both channels is better than −18 dB, and the two transmission zeros greatly enhance the channel selectivity. The low-frequency channel in Fig. 9(f) is located at 1.44 GHz, and the bandwidth is 150 MHz. The high-frequency channel bandwidth is 150 MHz, and the adjustment range is 2.21 GHz to 2.57 GHz. The in-band reflection of both channels is better than −16 dB, and the channel selectivity is improved obviously because of the two transmission zeros around the passband.

Table 3 shows the comparison in performance between the switchable and tunable triple-channel bandpass filter proposed in this paper and the multi-channel filters reported in the published literature. It can be seen from Table 3 that the filter proposed in this work is outstanding in terms of whether the channels are switchable and tunable, especially whether the three channels are independently adjustable.

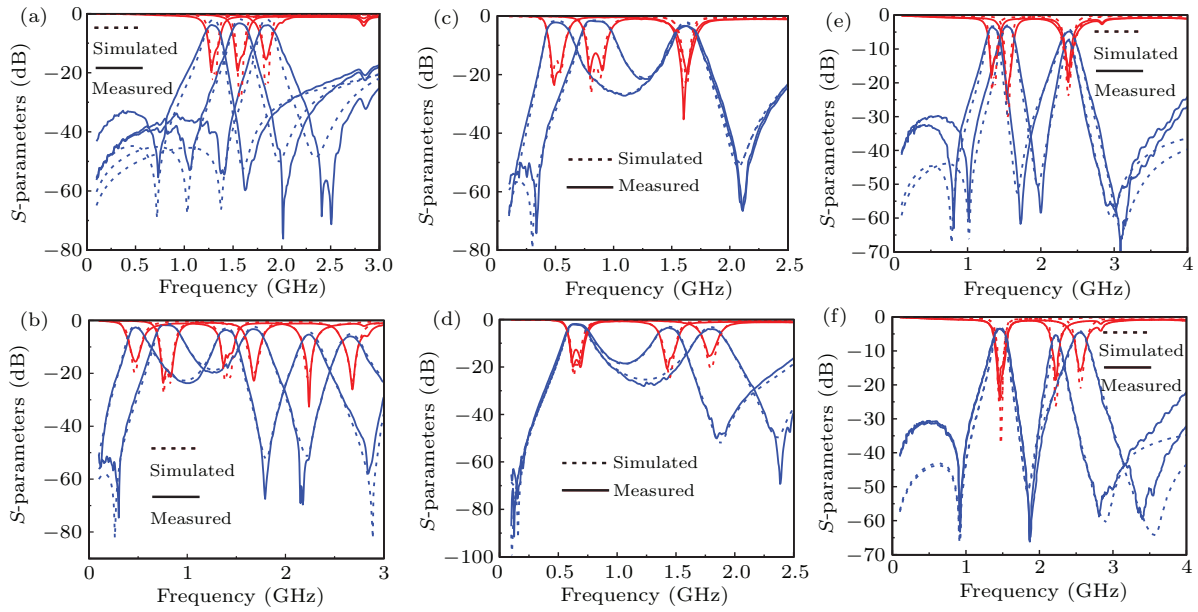


Fig. 9. Simulated and measured results for (a) D_1: OFF, D_2: OFF, single-channel; (b) D_1: ON, D_2: ON, triple-channel; (c) D_1: ON, D_2: OFF, dual-channel, channel 1 tunable; (d) D_1: ON, D_2: OFF, dual-channel, channel 2 tunable; (e) D_1: OFF, D_2:ON, dual-channel, channel 2 tunable; and (f) D_1: OFF, D_2:ON, dual-channel, channel 3 tunable.

Table 3. Comparison between our filter and reported reconfigurable filters.

Ref.	NoC	CF (GHz)	RL (dB)	SWA	TUA	TR (GHz)
[3]	4	1.54/2.45 3.58/5.2	better than 12	×	×/× ×/×	
[4]	2	2.33/4.9	better than 16	×	× /×	
[5]	2	1.35/3.7	–10/–17	×	√/×	1.2–1.5
[6]	2	0.837/2.4	–10/20	×	√/×	0.805–0.87
[7]	2	1.1/1.79	–10.1/–14.4	×	√/√	0.98–1.22 1.63–1.95
[8]	2	1.22/1.74	better than 10	×	√/√	0.99–1.44 1.5–1.97
[9]	2	1.95/2.45	–10.5/–12.9	×	√/√	1.7–2.2 2.2–2.7
[10]	2	0.9/1.79	–12/–11	×	√/√	0.77–1.02 1.57–2
[11]	2	1.44/2.29	better than 10	×	√/√	1.15–1.72 2.12–2.45
[12]	2	2.82/3.59	better than 16.5	×	√/√	2.55–3.08 3.33–3.84
[13]	2	0.79/3.23	better than 20	×	√/√	0.69–0.88 2.67–3.78
[14]	2	0.64/1.29	better than 12	√	√/√	0.55–0.72 1.17–1.4
[15]	2	1.27/2.12	–12/–14	√	√/√	0.76–1.78 1.6–2.63
[16]	2	0.8/0.96	better than 15	√	√/√	0.69–0.9 0.85–1.07
[17]	2	0.89/1.82	–18.8/–17.2	√	×/×	
Our	3	0.64/1.54, 2.46	better than 13	√	√/√/√	0.46–0.82 1.37–1.71 2.22-2.7

NoC: channel number; CF: channel frequency; RL: return loss; SWA: switchable; TUA: tunable; TR: tunable range.

4. Conclusions

The switchable and tunable triple-channel bandpass filter proposed in this paper realizes the free switching among single-channel, dual-channel, and triple-channel by loading varactors and switching diodes on the resonator, and each channel is independently adjustable. In addition, a rigorous rank criterion is proposed.

Acknowledgements

Project supported by the National Natural Science Foundation of China (Grant No. 61471094) and the Science and Technology Support Program of Sichuan Province, China (Grant Nos. 2019YFG0499 and 2020YFG0231).

References

[1] Chen L, Cheng Z X, Xu J M, Zang X F, Cai B and Zhu Y M 2014 *IEEE Opt. Lett.* **39** 4541
[2] Chen L, Liao D G, Guo X G, Zhao J Y, Zhu Y M and Zhuang S L 2019 *IEEE Frontiers of Information Technology & Electronic Engineering* **20** 591
[3] Zhang S X, Qiu L L and Chu Q X 2017 *IEEE Microw. Wirel. Compon. Lett.* **27** 974
[4] Ren B P, Ma Z W, Liu H W, Guan X H, Wang X L, Wen P and Ohira M 2019 *IEEE Trans. Microw. Theory Tech.* **67** 726
[5] Zhou L H, Ma Y L, Shi J, Chen J X and Che W C 2016 *IEEE Trans. Microw. Theory Tech.* **64** 4183
[6] Chen J X, Du M Z, Li Y L, Yang Y J, and Shi J 2018 *IEEE Transactions on Components, Packaging and Manufacturing Technology* **8** 113
[7] Chen Z H and Chu Q X 2016 *IEEE Microw. Wirel. Compon. Lett.* **26** 92
[8] Fan M Y, Song K J, Yang L and Gómez-García R 2021 *IEEE Trans. Microw. Theory Tech.* **69** 1365
[9] Chen F C, Li R S and Chen J P 2018 *IEEE Access* **6** 46058
[10] Huang X G, Zhu L, Feng Q Y, Xiang Q Y and Jia D H 2013 *IEEE Trans. Microw. Theory Tech.* **61** 3200
[11] Yang T and Rebeiz G M 2013 *IEEE Trans. Microw. Theory Tech.* **61** 3613
[12] Wei F, Zhang C Y, Zeng C and Shi X W 2021 *IEEE Trans. Microw. Theory Tech.* **69** 4029
[13] Pal B, Mandal M K and Dwari S 2019 *IEEE Microw. Wirel. Compon. Lett.* **29** 255
[14] Chen X, Yang T and Chi P L 2021 *IEEE Access* **9** 14216
[15] Lu D, Tang X H, Barker N S and Feng Y K 2018 *IEEE Trans. Microw. Theory Tech.* **66** 1215
[16] Cho Y H, Park C and Yun S W 2021 *IEEE Access* **9** 16967
[17] Xu J, Liu F and Feng Z Y 2020 *IEEE Trans. Microw. Theory Tech.* **68** 741